Islamic Azad University

Journal of Optoelectronical Nanostructures

Journal homepage: https://sanad.iau.ir/journal/jopn

Research Paper

Internal Quantum Efficiency in Gan/Ingan Multiple-Quantum-Well Light-Emitting Diodes under Temperature and Hydrostatic Pressure

Rajab Yahyazadeh[*1], Zahra Hashempour[1]

[1] Department of Physics, Khoy. C., Islamic Azad University, Khoy, Iran

Article History:

Received:	27.09.2025
Revised:	17.11.2025
Accepted:	18.11.2025
Published:	31.12.2025

Use your device to scan and read the article online

Keywords:
Internal efficiency,
Huang-Rhys factor,
Capture coefficient,
Multi-quantum well

Abstract:

This study used a numerical model to investigate the internal quantum efficiency in InGaN/GaN multiple-quantum-well light-emitting diodes (MQWLEDs) under varying temperatures and hydrostatic pressures. Our calculations demonstrated that a temperature change could increase the carrier capture coefficients, while a change in pressure could decrease them in the quantum well. It was further found that the carrier-LO phonon coupling of heavy holes made the smallest contributions to hole capture coefficients. Based on these results, radiative and non-radiative recombination (i.e., Auger and Shockley-Read-Hall) and carrier leakage current decrease with increasing pressure and increase with increasing temperature. Increasing pressure by 10 GPa increases the quantum efficiency, while increasing temperature in the range of 300-600K has the opposite effect, decreasing it. Comparing this model with other models and experimental data demonstrates the good validity of this model, particularly in light of the multiphonon model. Generally, increasing temperature has a negative effect and increasing pressure has a positive role on the internal quantum efficiency.

Citation: Rajab Yahyazadeh, Zahra Hashempour. Internal quantum efficiency in InGaN/GaN multiple-quantum-well light-emitting diodes under temperature and hydrostatic pressure. **Journal of Optoelectronical Nanostructures.** 2025; 10 (4): 36-63.

***Corresponding author:** Rajab Yahyazadeh
Address: Department of Physics, Khoy. C., Islamic Azad University, Khoy, Iran
Email: rajab951357@iau.ac.ir
DOI: https://doi.org/10.71577/jopn.2025.1219305

1. INTRODUCTION

For the past three decades, GaN-based semiconductors have contributed significantly to the improvement of performance photonic devices [1-4]. InGaN materials exhibit outstanding properties, including a high optical absorption, high velocity, high thermal stability, high mobility, and high resistance. [5-8]. All these properties make InGaN a good candidate for applications in high-temperature operation. Research efforts on InGaN light-emitting diodes, particularly under temperature and hydrostatic pressure, have increased significantly over the past two decades [5, 6, 9, 10, 11]. Therefore, it is essential to study their external and internal quantum efficiencies (IQE), which have been investigated through various theoretical models and experimental methods [12-15]. Estimating the total efficiency requires calculating the IQE, as the main source of the decrease in the total efficiency. Significant contributors to the IQE droop are non-radiative recombination, and carrier leakage [16, 17]. Various methods have been proposed for calculating the internal quantum efficiency in optoelectronic systems [12, 18-21]. In these works, radiative and non-radiative recombination coefficients are often considered as fitting parameters. One of the most famous models is the ABC model. In this work, the carrier density is assumed to be equal, while the total recombination coefficients (Auger, Shockley-Read-Hall (SRH) and radiative) are considered constant and independent of external perturbations. Therefore, to accurately calculate the internal quantum efficiency of optoelectronic devices, it is necessary to provide a comprehensive model that is well consistent with experimental data.

Considering the mentioned points, the present study aims to introduce a comprehensive model in which total recombination and their coefficients, the total injection, are investigated under external pressure and temperature without using parameter fitting. Given the breadth of the subject, in our previous works, we have separately investigated and calculated each of the non-radiative Auger and radiative currents independently [22, 23]. In this work, we calculate the total current by adding the Shockley-Read-Hall and leakage currents, providing a comprehensive analysis of these two components. The SRH recombination is one of the most effective process of the decrease in efficiency. [24, 25]. Different method (e.g. numerical and analytical) used to compute the SRH recombination. Piperk et al. calculated the relationship of the Shockley-Read-Hall coefficient on the electron concentration using ABC model [21]. Aurelin et al. computed the SRH coefficient through integrating the carrier overlap in the quantum well and the multi-phonon theory [26, 27]. Pristovesk et al. calculated the relationship

between the Shockley-Read-Hall coefficient and density of defects [28]. Also, the relationship of SRH on the carrier band energy and temperature in photonic devices computed by Bulashevich et al. and Shishehchi et al. [29, 30]. The hydrostatic pressure is used to adjust the wavelength of the laser diode [31]. In this work, the theory of multiphonon is used to investigate the carrier capture coefficients [32], as parameter dependent on the transition energy. In all studies conducted on photonic devices such as LEDs, the defects radius is constant. However, in this work, we study its relation on external perturbation. Furthermore, we investigated the effects of the total holes into the calculation capture coefficients.

2. CALCULATION MODEL

The sample studied in this work is similar to previous works. (Figure 1) [22,33]. To calculate the subband energy, the wave functions of electrons and holes, the Schrödinger and Poisson equations, as well as the 6×6 k.p method, have been used, respectively[22.34,35]. In this model, we consider the effect of pressure and temperature-dependent parameters to calculate radiative and non-radiative recombination [36, 37]. These parameters are the effective mass, phonon frequency, internal polarization fields, and dielectric constants. Total current density in MQW light emitting diode is [38]

$$IQE = NeL_w R_{rad} / \overbrace{\left(NeL_w[R_{SRH} + R_A + R_{rad}] + J_l\right)}^{J_{total}} \quad (1)$$

In this context, R_{SRH}, R_A, and R_{rad} refer to SRH, Auger, and radiative recombination, respectively; J_l is the carrier leakage current; and N_w and L_w are the number of quantum wells and well thickness, respectively. To better explain the working model, Fig. 2 presents a schematic illustration of the recombination components, along with the paths of carrier injection and leakage currents. Meanwhile, leakage currents exist outside these regions and toward the blocking layers of $In_{0.2}Ga_{0.8}N$. To calculate the efficiency, total recombination and leakage current must be calculated, as follows.

The non-radiative SRH recombination rate is calculated as [27, 30, 39, 40]:

$$R_{SRH} = \int_0^{L_{eff}} \frac{N_t c_p(z) p(z) c_e(z) n(z)}{c_p(z)[p_d + p(z)] + c_e(z)[n_d + n\ (z)]} (1 - \exp(\frac{E_{Fp}(z) - E_{Fn}(z)}{k_B T}) dz \quad (2)$$

where $n(z)=\sum_{i=1}^{20}(m_e^* k_B T/\pi\hbar^2)\psi_i^2(z)Ln\left[1+exp-(E_i-E_F)/K_B T\right)\right]$ is the electron density[32]. Additionally, m_e^* is the effective mass [32, 41]. Furthermore, $E_g(T,P)=E_g(0,0)+\beta P+\sigma P^2-\left(\alpha T^2\right)/(T+T_e)$ is the band gap [32]. The numerical values of the band gap constants (α, σ, and β) are listed in Table 1 [42]. $L_{eff}=(1/n(z))\int_0^{L_{InGaN}} n(z)zdz$ is the width of QW that can be calculated after calculation of electron density [43].

Where $p(z)=(m_h^* k_B T/\pi\hbar^2)\sum_{i=1}^{20}\sum_{\upsilon}^{3} ln\left[1+\exp(E_i-E_F)/(k_B T)\right]\left|g_i^{\upsilon}(z)\right|$ is the density of holes, in which $g_i^{\upsilon}(z)$, m_h^* and E_i the hole envelope function , mass and the subband energy. $g_i^{\upsilon}(z)$ is normalized such that $\sum_{\upsilon=1}^{3}\int_0^{L_{GaN}}\left|g_i^{\upsilon}(z)\right|^2 dz=1$ [44] . The effective masses of holes are obtained using the k.p method and ternary relation [45, 46]. In this work, the positions of the Fermi levels corresponding to electrons (E_{Fn}) and holes (E_{Fp}) are shown in Figure 1. The defect density is assumed to be $N_t=1.5\times10^{14}cm^{-3}$, which is similar to the work of reference 27.

Where c_e and c_p are the capture coefficients of the electron and holes. In this work, we investigated the electron capture coefficients, as the hole capture coefficients in the valance band is similar to the electron calculation method. Using Fermi's golden rule, c_e is expressed as follows [27, 32, 47]:

$$c_c(z)=\sum_{i,i',j} G_{ij}\times F_{ij}(16\pi^2 a_{ij}^3/\hbar)(\Delta E_{ij}-S_{ii',c}\hbar\omega_{LO})^2\left|\psi_{i,c}(z)\right|^2 \qquad (3)$$

In this model, the defects radius is $a_{ij}=\hbar/[2m_{ei}^*\Delta E_{ij}]^{1/2}$ [30]. Moreover, $\Delta E_{ij}=(E_{ij}-E_T)$ is the energy difference between the ith subband and trap level. In addition, $E_{ij}=E_i^e+E_j^h+E_g^{GaN}-E_b^{ij}-eF_W L_{eff}$ is the transition energy of the electron relative to the valence band subbandes [48]. In this relation, E_j^h and E_i^e are the subband energy of the holes and electron in the quantum well, respectively, and E_b^{ij} is the excitons bounding energy. Exciton energies are determined using the variability method. [49]. Moreover, F_w is the polarization electric fields

(spontaneous and piezoelectric) in the quantum well [42, 50]. In this model, the rule of selection is no longer imposed. The deep traps energy (E_T) in the QW is a tenths of volt above the median of the transition energy and toward the valence band [27, 51]. Additionally, the median of the transition energy is the position of the deep traps energy, considering the median of the transition energy for the traps energy ($E_T = E_{ij}/2$). Deep trap have a negative impact on the efficiency of InGaN/GaN LEDs. [52]. In the work, the first subband transition energy of the heavy holes $In_{0.4}Ga_{0.6}N$ QW (at 0 GPa and 300K) is 2.38 eV [32]. The transition energy in the middle of band gapes is 1.2 eV. Additionally, $\omega_{LO}(T) = \omega_{LO} + \Delta\omega_e(T) + \Delta\omega_s(T) + \Delta\omega_d(T)$ is the temperature-dependent LO-phonon frequency [53, 54]. Here, $\Delta\omega_e(T) = -\omega_{LO}(0)\gamma\int_0^T \left[\alpha_c(T') + 2\alpha_a(T')\right]dT'$ is the thermal expansion contribution (volume change), where γ is the Grüneisen parameter whose numerical values are listed for GaN and InN in Table 1. Also, $\alpha_c(T)$ and $\alpha_a(T)$ are the coefficients for temperature dependent of linear thermal expansion, respectively, whose temperature-dependent relationships are in Table 1. In addition, $\Delta\omega_S(T) = \varepsilon(T)[2a - b(2C_{13}/C_{33})]$ is the contribution of strain induced to the phonon frequency. This variation is due to a inconformity between the GaN (or InN) and sapphire substrate. In this equation, $\varepsilon(T) = (\varepsilon_g + 1)[(1 + \int_{T_g}^{T} \alpha_{a,S}(T')dT') / (1 + \int_{T_g}^{T} \alpha_a(T')dT')]$ is the temperature-dependent in-plain strain. $\alpha_{a,S}(T)$ and $\alpha_a(T)$ are the temperature dependent in-plain linear expansion coefficients, whose temperature-dependent relationships are in Table x. Moreover, ε_g is the residual strain InN(or GaN) at its growth temperature T_g of 500 K. In this model, the residual strain ε_g at the growth temperature T_g is equal to zero [54]. In this work, the third and fourth order terms in the nonharmonic Hamiltonian and the symmetric decays of the center-region phonons into two ($\omega_{LO}(0)/2$) and three ($\omega_{LO}(0)/3$) phonons are considered, the term $\Delta\omega_d(T)$ can be expressed as [54]:

$$\Delta\omega_d(T) = \Delta\omega_{d1} + \Delta\omega_{d2} = M_1[1 + 2n(T, \omega_{LO}(0)/2)] + M_2[1 + 3n(T, \omega_{LO}(0)/3) + 3n^2(T, \omega_{LO}(0)/2)] \quad (4)$$

where M_1 and M_2 are constant values, the numerical values of which are in Table 1. The numerical values of the other coefficients associated with M_1 and M_2 in the quantum well are obtained by the ternary relation [55]. In addition,

$\omega_{LO}(T,P)=\omega_{LO}(0)\exp(\gamma_{LO}P/B_0)$ is the LO- phonon frequency [56]. Numerical values of γ_{LO} and B_0 are in Table 1 [56].

The strength of carrier-LO phonon coupling is characterized by HRF whose relationship is shown as follows (see Appendix A) [57, 58]:

$$S_{ii',c}=\sum_q\left(e^2/2V_0\hbar\omega_{LO}\right)\left[(1/\varepsilon_\infty)-(1/\varepsilon_0)\right]\times q^2\Big/\left(q^2+\lambda_s^2\right)^2 \left\{\begin{matrix}n_q+1\\ n_q\end{matrix}\right\}\delta\left(k_P-k_P',q_P\right)\left|\int e^{-iq_\perp z}\psi_{ic}^*(z)\psi_{i'c}(z)dz\right|^2 \quad (5)$$

where q, V_0 and n_q are the phonon wave vector, phonon occupation factor and the unit cell volume, respectively[36]. In this study, $\lambda=(4\pi e^2[n+p]/\varepsilon_{InGaN}k_BT)^{1/2}$ is the reverse screening lengths [59, 60]. Furthermore, $I_{c-ph}=\int\psi_{ic}^*(z)\psi_{i'c}(z)e^{-iq_\perp z}dz$ is the scattering integral in the quantum well.

where G_{ij} is the subsidiary function and is shown as follows [27, 61]:

$$G_{ij}=(1/(\hbar\omega_{LO}\sqrt{2\pi\chi_{ij}}))[\xi_{ij}/(P_{ij}+\chi_{ij})]^{P_{ij}}\exp(\chi_{ij}-(2n_q+1)S_{ij}+\Delta E_{ij}/2kT) \quad (6)$$

where $P_{ij}=\Delta E_{ij}/\hbar\omega_{LO}$ is the number of phonons in scattering process, $\xi_{ij}=2S_{ij}[\bar{n}(\bar{n}+1)]^{1/2}$, and $\chi_{ij}=(P_{ij}^2+\xi_{ij}^2)^{1/2}$. Furthermore, F_{ij} is a function that depends on the electric charge of the carriers centers. The value for carriers charge has been calculated by Kang et al. [61.In this work for the simplicity, we ignore charge effects and, following Refs.27, 47, and 60, we set $F_{ij}=1$.

In the ABC model the carrier densities are equal [21], the non-radiative recombination of SRH is obtained by integrating on effective well width. In this state, Shockley-Read-Hall constant ($A=R_{SRH}/n$), which is as follows:

$$A=N\int_0^{L_{eff}}N_t\overbrace{\frac{c_e(z)\times c_p(z)}{c_e(z)+c_p(z)}}^{C_{eq}}(1-\exp(-\frac{E_{Fn}(z)-E_{Fp}(z)}{k_BT})dz \quad (7)$$

By determining the effective well width (L_w), Shockley-Read-Hall coefficient (A), density of carriers and the number of QWs (N), the SRH current ($J_{SRH}=NqL_wAn$) is calculated [62].

In this model, the Auger recombination (AR) is obtained from the Golden Fermi function according to the following relationship, which is as follows [23, 63, 64]:

$$R_A = \frac{1}{4\pi\hbar L_{eff}}\left(\frac{e^2}{4\pi\varepsilon_w}\right)^2\left(\frac{4\pi}{(2\pi)^3}\right)^2 \times \sum_{allE_z}\int\int\int\int \overbrace{|\boldsymbol{k}-\boldsymbol{k}'|^{-2} A_k^2}^{M}\delta(\boldsymbol{k_1}-\boldsymbol{k_{1'}}+\boldsymbol{k_2}-\boldsymbol{k_{2'}})P_{1,1',2,2'}\delta(E)d^2\boldsymbol{k}_1 d^2\boldsymbol{k}_{1'} d^2\boldsymbol{k}_2 d^2\boldsymbol{k}_{2'} \quad (8)$$

Where, $\delta(E)$, M, A_k are the energy conservation , matrix element for interaction potential of carriers, and the overlap integral, respectively [63]. Further, $P_{1,1',2,2'} \approx f_{v1} f_{c1'} f_{v2}[1-f_{v2'}]$ account for sate occupations. Additionally, k and k' are the in-plain wave vectors of two dimensional, respectively. In this study, we calculate three AR, namely the CHHL, CHHS and CCCH processes, independently so that we can obtain the total recombination through them. Also, the effective Auger coefficient after calculating the AR is given by [64].

$$C_w(InGaN) = \overbrace{[R_w(CHHS)/\bar{p}_w{}^2\bar{n}_w]}^{C_w(CHHS)} + \overbrace{[R_w(CHHL)/\bar{p}_w{}^2\bar{n}_w]}^{C_w(CHHL)} + \overbrace{[R_w(CCCH)/\bar{n}_w{}^2\bar{p}_w]}^{C_w(CCCH)} \quad (9)$$

where $\bar{p}_{w,b}$ and $\bar{n}_{w,b}$ are the medium hole and electron density inside the barriers(b) and wells (w).

The radiative recombination (RR) rate is given by [40, 65]:

$$R_{rad} = (np - n_i^2)\overbrace{\frac{2\pi}{n_i^2 h^3 c^2}\int_{E_g^{11}}^{\infty} n_{eff}^2 \alpha(E) e^{-E/k_B T} E^2 dE}^{B} \quad (10)$$

Here B and n_i are the RR coefficient and intrinsic densities of the carriers respectively. The optical absorption is calculated as [66, 68]:

$$\alpha_W(E') = \frac{\pi\hbar q^2}{E'\varepsilon_0 m_0^2 c n_{eff}} \times \sum_{i,j}\int_{E_{g,w}}^{E_{g,b}} D_{r,ij}^{2D}|Mij|^2\left(f_{i_v} - f_{j_c}\right)L\left(E' - E_{ij}\right)dE_{ij} \quad (11)$$

Where $L(E'-E_{ij}) = (\Gamma_{hom}^2)/2\pi[(E'-E_{ij})^2 + \Gamma_{hom}^2]$, $D_r^{2D} = m_{r,ij}/\pi\hbar^2$, $\left|M_{ij}\right|^2$ are the Lorentzian function, the reduced density and $\left|M_{ij}\right|^2$ is the transition strengths. Where Γ_{hom} is the linewidth (related to scattering of carriers and phonons) (see Appendix A) [56, 69]. The relaxation time ($\tau_{in} = \hbar/[\Gamma_{cjk}(E) + \Gamma_{vjk}(E)]$) is

obtained from Eqs. (A4) and (A1) (see Appendix A). Finally, n_{eff} is the refractive index [39].

$J_{le} = q[(NL_{eff} N_w / \tau_w) + (d_g - NL_{eff}) N_b / \tau_b]$ is the leakage current of electrons, especially at high temperatures [57,69,71]. In this relation, $N_w = N_{c,w} \exp[(E_{Fn} - \Delta E_c) / k_b T]$ and $N_b = N_{c,b} \exp[(E_{Fn} - \Delta E_c) / k_b T]$ denote the concentration of electrons in thermal equilibrium in the QW and barrier, respectively; d_g is the thickness of the MQW layer; and ΔE_c is the energy difference above the QW from the first subband (with the highest density). Also, $\tau_{in} = [(2\pi m_i^* L_w^2) / k_B T] \exp[(E_{Fi} - E_i) / k_B T]$ is the lifetime of the electrons above the barrier and wells, respectively [72]. The hole leakage current relationship is similar to the electron leakage current, in which we must replace the hole variables with the electron variables in these relationships.

3. RESULTS AND DISCUSSION

The internal quantum efficiency is obtained after solving all the paramours of recombination and leakage current. To calculate the recombination and leakage current, first calculate the bands profile. Bands profile for carriers are shown in Fig. 1a. To calculate variables of the light-emitting diodes, 1.5 V was applied to p-GaN region (Fig. 1b).

Fig. 3 illustrates the relationship of polarization and QW depth on temperature and hydrostatic pressure. As shown in Fig. 3, increasing the temperature by 300K (relative to room temperature) decreased QW depth and polarization density by 45 meV and $1.2\mathrm{m}^{-2}$, respectively (Fig. 3a) . An increasing the temperature altered the lattice constant, leading to a change in position of charges and decreasing polarization charge density (inset of Fig. 3a). Similarly, an increase in temperature decreased the centers of charges, thereby increasing the Coulomb interaction of carriers. By increasing the temperature by 600 K, the energy of first subband decreased by 18 meV. It also decreased carrier density and quantum confinement. As shown in Fig. 3b, increasing the hydrostatic pressure by10 GPa increases QW depth and polarization density by 65 meV and $1.4\mathrm{m}^{-2}$, respectively. According to Fig. 3, the effect of hydrostatic pressure on polarization and QW depth is exactly the opposite of the behavior of temperature on quantum well depth and polarization.

Among of the important parameters for computing the a_{ij}, Auger overlap integral, capture and optical absorption coefficients are the transition energy and ΔE_{ij} . In this work, we calculate only E_{ij} of the first subband so that the other

similar trend under external perturbations. The transition energy of first subband $(E_{11}^{e,hh})$, and $\Delta E_{11}^{e,hh}$ versus external perturbation is according to Fig. 4. Dependence on the temperature and pressure of E_{ij} and ΔE_{ij} is according to Fig. 4. By increasing the temperature up to 300K, E_{ij} and ΔE_{ij} decreased by 0.38 eV and 0.19 eV, respectively (Figs. 4a). In addition, those parameters by increasing the pressure by10 Gpa, increased by 0.43 eV and 0.22 eV (Figs. 4b). Also, temperature dependence of parameters in relation E_{ij} could change transition energy, which are F_W, E_i^e, E_j^h, E_g^{GaN}, E_b^{ij} and L_{eff}. The dependence of these parameters on pressure and temperature has been investigated in our previous work [22]. According to the obtained data (Figs. 4a and 4b), for an increase of 300°K in temperature and 10 GPa in hydrostatic pressure, the exciton energy increased by 8 meV and decreased to 8.8 meV, respectively. For illustration of localization under eternal perturbation, the wave function of carriers is plotted versus distance in Fig. 4. By increasing the temperature to 300K, the pick of Ψ_e decreased from $1.78\times10^4 m^{-1/2}$ to $1.54\times10^4 m^{-1/2}$ and was delocalized. Furthermore, for heavy holes, the pick of Ψ_{HH} decreased from $3.1\times10^4 m^{-1/2}$ to $2.56\times10^4 m^{-1/2}$, indicating a decrease in quantum confinement and localization and thereby more overlap of wave functions between carrier (inset of Figs. 5a). By increasing the temperature up to 600K, the wave functions overlap increased $8.5\times10^2 m^{-1/2}$. Therefore, more overlap indicates an increase in the Coulomb energy of the carriers (electron and holes), suggesting that E_b^{ij} increases by increasing temperature (inset of Fig. 4a). Figs. 5b displays that the carrier and overlap wave functions region, with increasing pressure, is exactly the opposite of their behavior with increasing temperature. Therefore, increasing the pressure by10 GPa, the overlap region decreased $7.2\times10^2 m^{-1/2}$; thus, decrease in the Coulomb interaction of the carriers, suggesting that E_b^{ij} decreases by increasing pressure (Fig. 4b).

Effective mass of carriers is the important parameter in calculating the point defects radius, Auger overlap integral, capture and optical absorption coefficients, which requires calculating and drawing the band structure of hole carriers, as shown in Fig. 6a and 6b. From these figures, band edges of heavy hole are constant and independent of temperature and hydrostatic pressure. As a result, m_{hh}^* is not effective in recombination. However, the effective mass of LH and SO hole changes with temperature and pressure, which is impressive in

recombinations. Hence, the temperature and hydrostatic pressure will be impressive on these holes when calculating the recombinations.

LO-phonon frequency is the important parameter to calculate the n_q and Huang-Rhys factor, which depends on temperature and pressure. In analyzing the pressure and temperature dependence of phonon frequencies, it is necessary to investigate their origin, which is related to the polarization fields (F_w). The change in polarization under the influence of temperature and pressure causes changes in the polarization fields. These changes are as shown in Figs 7a and 7b. By increasing pressure by 10 GPa, the polarization field increases in the MQW region by 0.77 MV/cm, and a temperature rise in the range of 300-600 K reduces this field to 0.57 MV/cm. An increase in the polarization field charge density causes an increase in electron and hole density (Figs. 7c-7f). The density of carriers increase in the MQW region is $0.78\times10^{18}cm^{-3}$ and $0.66\times10^{18}cm^{-3}$ for holes and electrons, respectively. But with increasing temperature up to 600, the average density of holes and electrons decreases to $0.52\times10^{18}cm^{-3}$ and $0.68\times10^{18}cm^{-3}$, respectively. Furthermore, changes in hydrostatic pressure altered the distance between charge centers, thereby modifying σ (Figs. 3a and 3b), which in turn increased the F_w and LO-phonon frequency.

Another parameter in calculating the capture coefficient is the $\omega_{LO}(T)$, which also depend on $\Delta\omega_e(T)$, $\Delta\omega_s(T)$, $\Delta\omega_{d1}(T)$ and $\Delta\omega_{d2}(T)$ contributions for LO-phonon frequency according to Fig. 8a. Increasing the temperature by 300K (relative to room temperature at 0GPa) reduced the LO phonon frequency by 14 cm^{-1}. Comparison with experimental data from reference 53 confirms the model. Also, an increase in pressure by 10 GPa (at 300K) increased $\omega_{LO}(T)$ by 21 cm^{-1} (Fig. 8b).

The temperature and hydrostatic pressure dependence of Huang-Rhys factors is as shown in Fig. 9a. By increasing the pressure by 10 GPa, the reduction rate in Huang-Rhys factor was 0.54 and 0.23 for total holes and electron, respectively (Fig. 9b). Besides, Huang-Rhys factors increased with increasing temperature. This increase (Fig. 9b) related to the decrease in the confinement of electron and holes in quantum wells with increasing temperature. The increase in the confinement of electron and holes in quantum well increased the coupling of LO phonons with carriers, thereby increasing the Huang-Rhys factors with increasing temperature. But Huang-Rhys factors decreased with increasing hydrostatic pressure, which is related to confinement in quantum wells.

As a result, from Eq. (3), ce and cp are calculated (Fig. 10). As shown in Fig.10, the c_e and c_p increased with increasing temperature (Fig. 10a). This increment was related with an increase in the overlap and the coupling of LO phonons with

carriers (Figs. 5 and 9). Due to the low density of electrons compared to holes (e.g., hh and lh), c_e was lower than c_p. The equivalent capture coefficient (c_{eq}) in Eq. (7) is an effective parameter to calculation of SRH coefficient. By increase temperature up to 600K could increment the c_{eq} to 1.6 m^2s^{-1}. Furthermore, center of equivalent capture coefficients is located in a position of 47 nm, this position (47nm) moved toward the position of the holes by 0.12 nm. In addition, increasing the pressure could reduce the c_{eq} and moved toward position of the electrons by 0.16 nm (Fig. 10b).

Finally, the Shockley-Read-Hall recombination rate values were calculated by Shockley-Read-Hall coefficients (Figs. 11). As showen Fig.11 increasing the temperature in the range of 300-600K (at 0 GPa) could increase the value of Shockley-Read-Hall recombination up to $0.18\times10^{26} cm^{-3}s^{-1}$ (Figs. 11a). Additional, an increase in hydrostatic pressure caused lower the value of Shockley-Read-Hall recombination up to $0.25\times10^{26} cm^{-3}s^{-1}$ (Figs. 11b). Auger and radiative recombination and their coefficients are fully explained in Refs. 22 and 23. Their dependence on temperature and pressure is shown in Figs. 12 to 13. According to Figs. 12 to 13, pressure causes a decrease in recombination, while temperature causes an increase in recombination.

Table 2 presents the recombination coefficients calculated in this work, numerical value of these coefficients were compared with values from Refs. 79-82. Numerical value of these coefficients illustrated that the recombination coefficient in the quantum well is closed to value in earlier literatures.

The carrier leakage current is one of the variable used in internal quantum efficiency. The leakage current at different temperatures and pressures is as shown in Fig. 14. As explained in Fig. 3, increasing the pressure causes the quantum well of the carriers to become deeper. As a result, it will increase the quantum confinement and reduce the carrier leakage. Conversely, increasing the temperature will reduce the well depth and quantum confinement, thereby increasing the leakage current.

IQE can be determined by calculating all radiative and non-radiative recombinations as well as leakage current. As shown in Fig. 15, increasing pressure increases the IQE, while increasing temperature decreases it.

By applying an external voltage of 1.5 V (Fig. 1), the injection current density resulting from recombination and leakage currents increases to 180A/cm². In this case, for an increase pressure up to10 GPa, the quantum efficiency increases by 5%, and for a temperature change of 300K, it decreases by 4%. In Fig. 15, the maximum efficiency value is at a total current density of 7.5 A/cm². To verify the validity of the working model for calculating efficiency, we compared it with the work done by previous researchers, as shown in Fig. 16. It is of note that this

figure applies to a single quantum well with the characteristics of the structure described in Ref. 21. The figure also supports that our working is in agreement with the experimental data without fitting parameters. Additionally, the closeness of these models to the experimental data is explained by the fact that these works considered the recombination coefficient as fitting parameters.

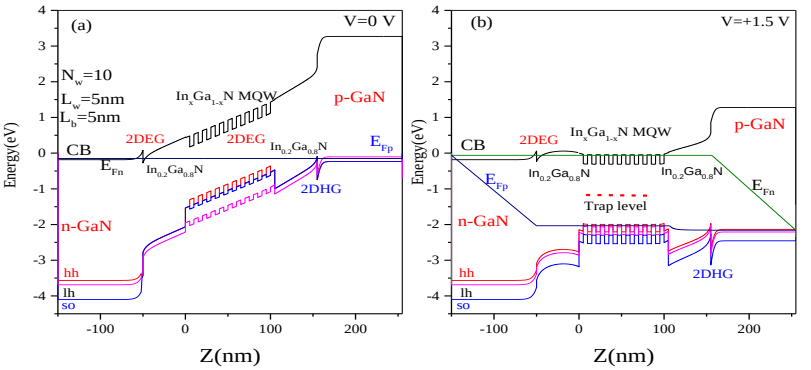

Fig. 1. The bands energy of electron (CB), heavy-hole (hh), light-hole (lh), and split-off hole (so) band in InGaN/GaN MQWLD versus distance for (a) 0V and (b) 1.5V. which m=0.3, 0.4 for barriers wells, respectively

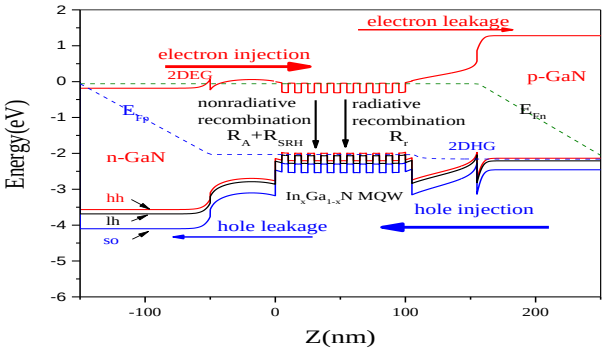

Fig. 2. Schematic illustration of InGaN/GaN LED recombination components (Radiative, Auger and SRH) along with the paths of carrier injection and leakage currents

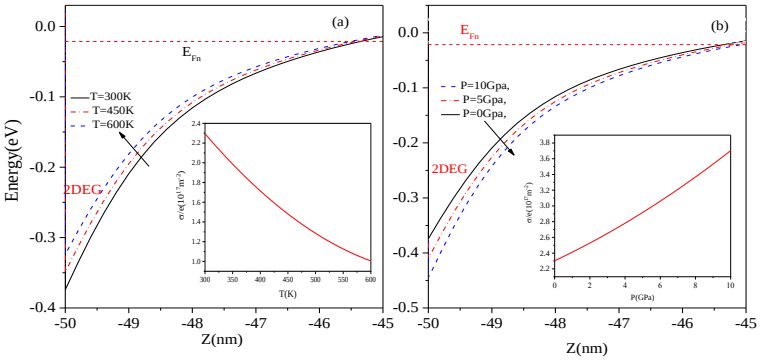

Fig. 3. The conduction band energy versus the distance under different temperature (a) and hydrostatic pressure (b); the insets illustrates the polarization charge density (σ/e)

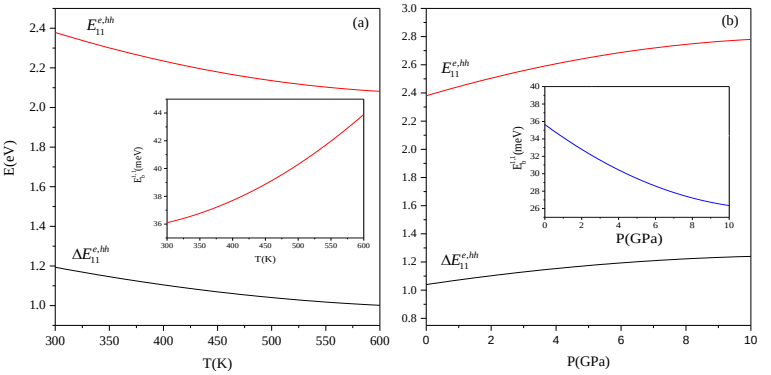

Fig. 4. The transition energy, and versus temperature (a) and pressure (b) for InGaN/GaN MQWLEDs; the insets represents the exciton binding energy versus temperature (a) and pressure (b)

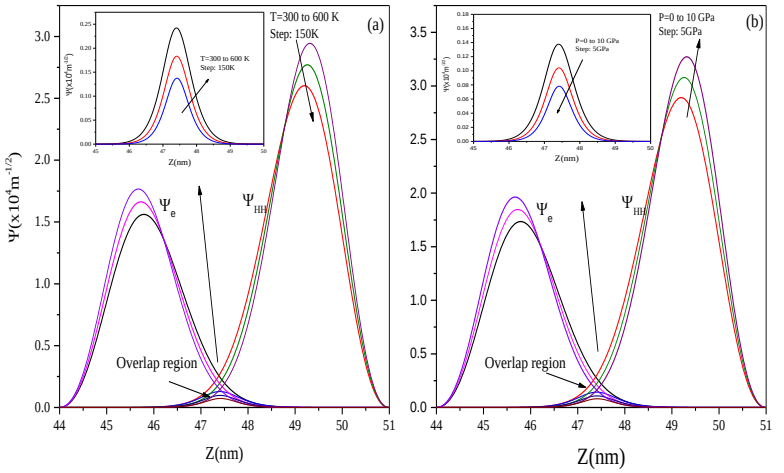

Fig. 5. The wave function of first subband carriers (heavy hole and electron) as a function of distance for InGaN/GaN MQWLEDs under temperature (a) and pressure (b). The insets demonstrate the changes of overlap region versus temperature (a) and c pressure (b)

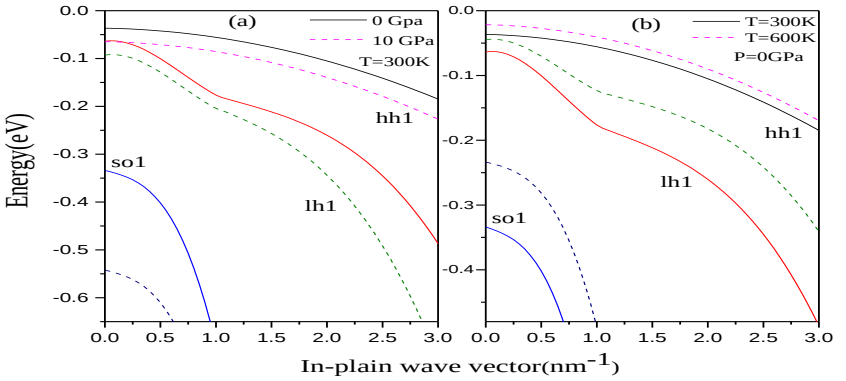

Fig. 6. The valence band of holes versus in-plain wave vector for QW $In_{0.4}Ga_{0.6}N$ under different hydrostatic pressure (a) and temperature (b)

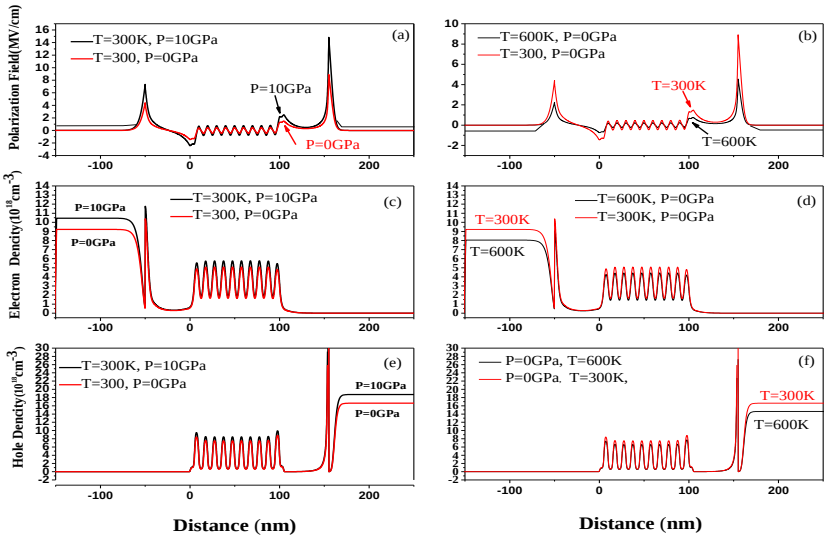

Fig. 7. Polarization field, electron and hole density of InGaN/GaN MQWLED versus distance under different temperature and hydrostatic pressure

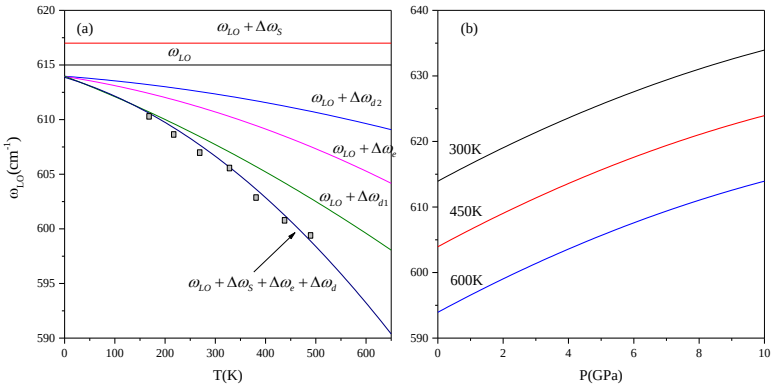

Fig. 8. LO phonon frequency versus temperature (a) and pressure (b) forInGaN/GaN MQWLED. Dotes represented the experimental data from reference 53

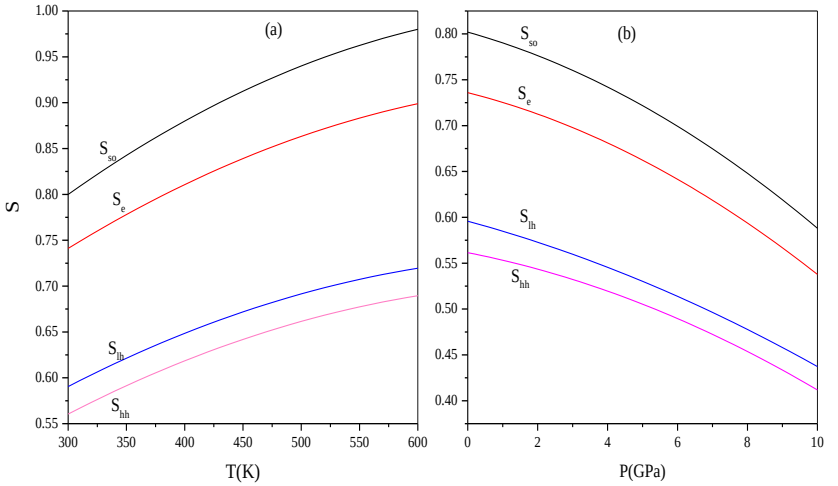

Fig. 9. Huang-Rhys factor (dimensionless) versus temperature (a) and hydrostatic pressure (b) in InGaN/GaN MQWLED

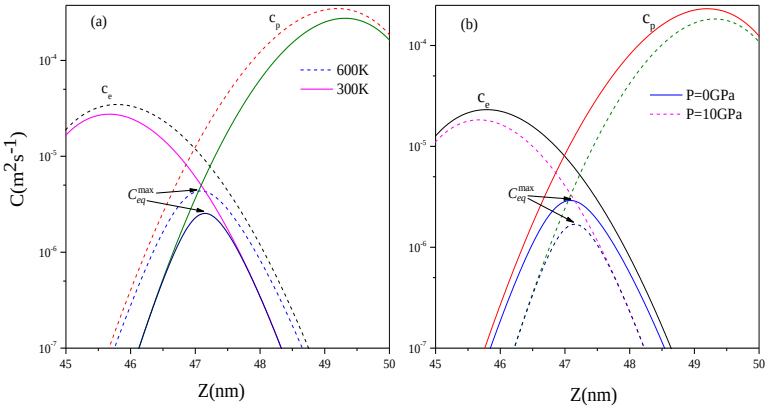

Fig. 10. Capture coefficients of electrons (ce), holes (cp), and equivalent (ceq) versus distance under temperature (a) and pressure (b)

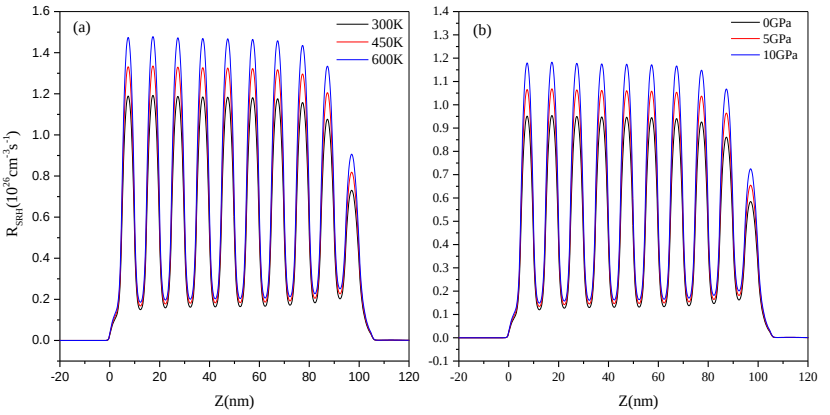

Fig. 11. Shockley-Read-Hall recombination rate of MQW region for InGaN/GaN LED versus distance under different temperature (a) and hydrostatic pressure (b) levels

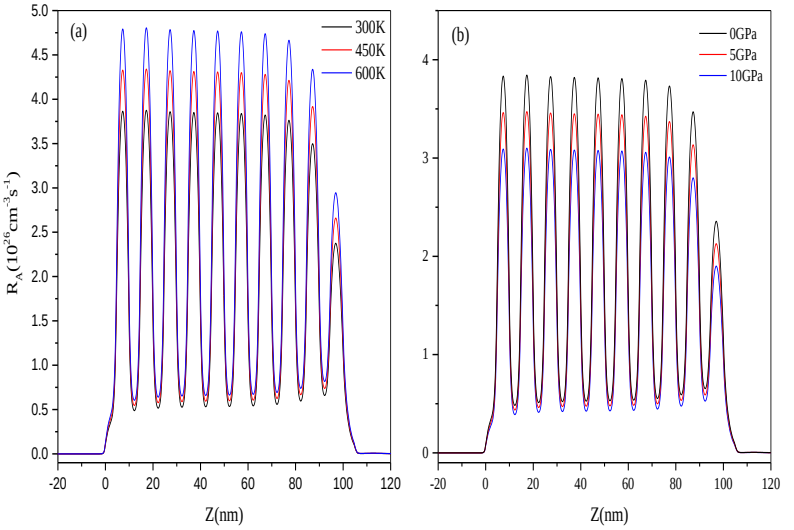

Fig. 12. Non-radiative Auger recombination rate of MQW region for InGaN/GaN LED versus distance under different temperature (a) and hydrostatic pressure (b) levels

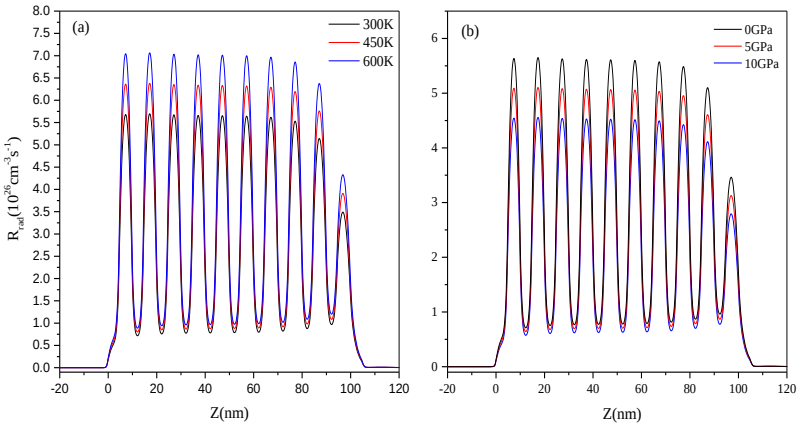

Fig. 13. Radiative recombination rate of MQW region for InGaN/GaN LED versus distance under different temperature (a) and hydrostatic pressure (b) levels

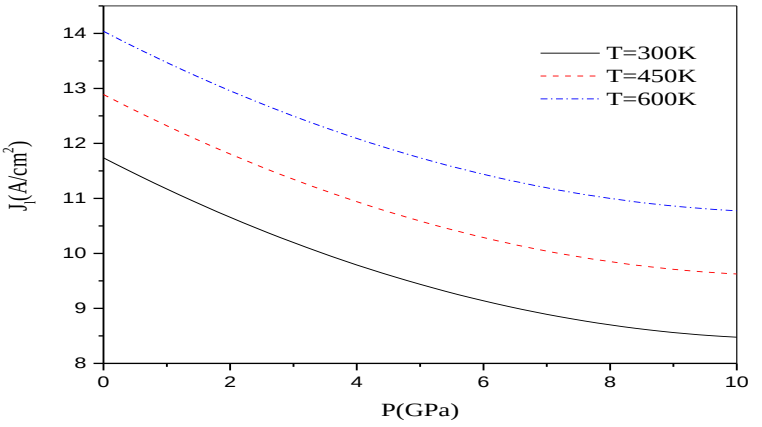

Fig. 14. Carrier Leakage current density for InGaN/GaN MQWLED versus different hydrostatic pressure and temperatures

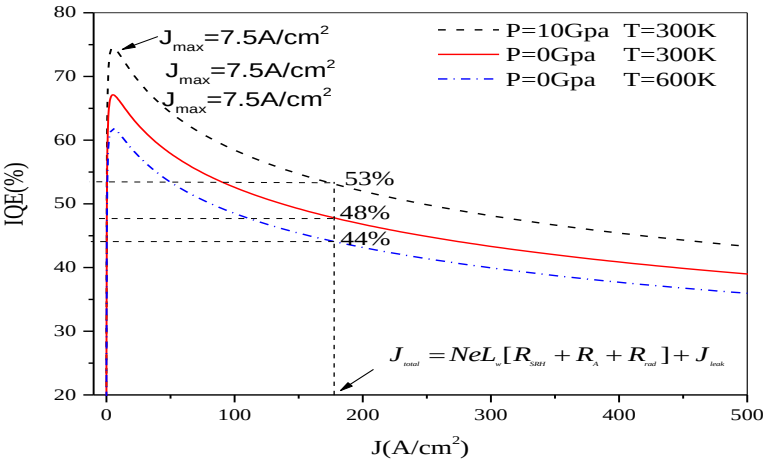

Fig. 15. Internal quantum efficiency versus current density under different temperatures and pressures in InGaN/GaN MOWLEDs

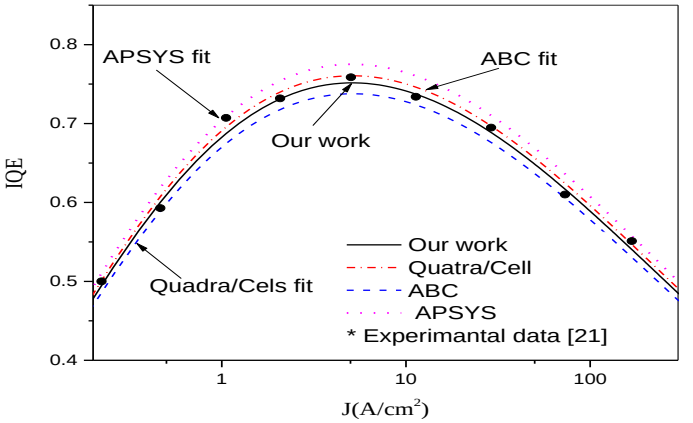

Fig. 16. Internal quantum efficiency versus current density, dotes are experimental data and different lines are models of the single quantum well InGaN/GaN LED

Table 1. Parameters and physical constant for InN and GaN

Parameters(unit)	GaN	InN	Refs.
$E_P^{\Gamma}(eV)$	14.0	14.5	[42]
$E_g^{\Gamma}(0K, 0GPa)$	3.42	0.7	[42]
$\Delta_{SO}(eV)$	0.014	-0.001	[42]
$\beta(meV.GPa)$	31.8	16	[78]
$\delta(meV.GPa^{-2})$	-0.23	-0.02	[78]
$\alpha(10^{-3}eVK^{-1})$	0.909	0.245	[42]
$T_e(K)$	830	624	[42]
ε_∞	5.39	6.7	[72]
$\omega_{LO}(cm^{-1})$	731.51	621.53	[74]
$C_{13}(GPa)$	103	92	[74]
$C_{33}(GPa)$	405	224	[74]
$B_0(GPa)$	190	136	[56]
γ_{LO}	1.08	126	[56]
$M_1(cm^{-1})$	2.80	-0.37 ± 0.05	[54,75]
$M_2(cm^{-1})$	0.15	-0.27 ± 0.14	[54,75]
$\alpha_c(10^{-6}K^{-1})$	3.17	2.165+0.00269T	[45,75,76]
$\alpha_a(10^{-6}K^{-1})$	5.59	2.134+0.00608T	[54,75,76]
$\alpha_{a,S}(10^{-6}K^{-1})$	7.5	0.943+0.00962T	[54,75,76]
$a(cm^{-1})$	-660	-610	[54, 77]
$b(cm^{-1})$	-1140	-875	[54, 77]

Table 2. Recombination coefficients reported in a number of works in InGaN/GaN MQW LED at 300K and P=0GPa

References	A($10^7 s^{-1}$)	B($10^{-11} cm^3 s^{-1}$)	C($10^{-30} cm^6 s^{-1}$)
This work	2.3	1.4	1.2
Zhang et al.[79]	1.0	2.0	1.5
Shen et al.[80]	5.4	2.0	2.0
Meneghini et al .[81]	2.3	1.0	1.0
Laubsch et al.[82]	0.47	0.12	0.35

4. CONCLUSIONS

This study investigated the internal quantum efficiency of InGaN/GaN MQWLEDs under varying temperatures and hydrostatic pressures. The results showed that that increasing the temperature in the range of 300-600 K led to increase the Huang-Rhys factor by up to 0.17 and 0.48 for electrons and holes in quantum wells, respectively. Additionally, increasing the hydrostatic pressure to 10 GPa led to decrease the Huang-Rhys factor by up to 0.22 and 0.53 for electrons and holes, respectively. On the other hand, increases in temperature lead to an

increase in the capture coefficients of carriers, while increasing pressure reduces them. By applying an external voltage of 1.5 V, the injection current density resulting from recombination and leakage currents increases to 180A/cm². In this case, applying pressure up to 10 GPa, the quantum efficiency increases by 5%, and for a temperature change of 300K, it decreases by 4%. Our numerical model provided the origin of the all recombination changes under temperature and pressure in LEDs. Finally, the performance of the light-emitting diodes is better when Auger and SRH recombination and leakage current are lower. Therefore, temperature and hydrostatic pressure play a negative and positive role in the IQE of these LEDs.

APPENDIX: HUANG-RHYS FACTOR

The carrier-phonon scattering of linewidth is obtained from one-particle Green's functions. The carrier-carrier scattering linewidth is given by [57]:

$$\Gamma_{njk_{\parallel}}^{c-c}=\pi\sum_{n'=c,v}\sum_{k',p}\sum_{i,j}\delta\left(E+E_{n'ip_{\parallel}}-E_{nj'k_{\parallel}}-E_{n'i'p'_{\parallel}}\right)\times\left|V_{nm}(k_{\parallel}k'_{\parallel},ii',jj')\right| \\ \times[f_n\left(E_{nj'k_{\parallel}}\right)f_{n'}\left(E_{n'i'p'_{\parallel}}\right)\left\{1-f_{n'}\left(E_{n'ip_{\parallel}}\right)\right\}+\left\{1-f_n\left(E_{nj'k'_{\parallel}}\right)\right\}\left\{1-f_{n'}\left(E_{n'ip'_{\parallel}}\right)\right\}f_{n'}\left(E_{n'ip_{\parallel}}\right) \tag{A1}$$

where n is the conduction or valence bands, i', i, j', and j are the subband of the QW structure. The matrix element of carrier-carrier interaction V_{nm} in QW is as follows

$$V_{nm}(k_{\parallel}k'_{\parallel},ii',jj')=\frac{e^2}{2\varepsilon_{GaN}A}\frac{\delta\left(k_{\parallel}-k'_{\parallel},p'_{\parallel}-p_{\parallel}\right)}{\sqrt{\lambda_s^2+\left|k_{\parallel}-k'\right|^2}} \\ \times\iint\phi^*_{nj'}(z_1)\phi_{nj}(z_1)\phi_{n'i'}(z_1)\phi^*_{ni'}(z_2)\times\exp(-|z_1-z_2|\sqrt{\left|k_{\parallel}-k'\right|^2+\lambda_s^2}\,dz_1dz_2 \tag{A2}$$

where A is the interface area of the sample, the z-axis is perpendicular to the well interface and the δ represents in-plain (parallel to the well interface) momentum conservation. $\phi_{nj}(z_1)$, is the wave function of a carrier. λ_s, is the inverse screening length and is calculated as [57]:

$$\lambda_s^2=\frac{e^2}{\pi^2\hbar^3\varepsilon_{GaN}}\sum_j[m_{cj}f_c\left(E_{cj}\right)\sqrt{m_{cj}E_{cj}}+m_{vj}f_v\left(E_{vj}\right)\sqrt{m_{vj}E_{vj}}] \tag{A3}$$

where m_{vj} and m_{cj} are the effective masses of holes in the valence (v) band and electrons in conduction (c) band. Llinewidth for carrier-longitudinal optical (LO) is calculated as [57]:

$$\Gamma_{njk_{\parallel}}^{c-ph} = \pi \sum_{k_{\square}'} \sum_{j'} \left| P_n\left(k_{\parallel} k_{\parallel}', jj'\right) \right|^2 \times \\ \times \delta\left(E_{nj'k_{\parallel}'} - E + \hbar\omega_{LO}\right)\left\{n_q + 1 - f_n\left(E_{nj'k_{\parallel}}\right)\right\} + \delta\left(E_{nj'k_{\parallel}'} - E - \hbar\omega_{LO}\right)\left\{n_q - f_n\left(E_{nj'k_{\parallel}'}\right)\right\} \quad \text{(A4)}$$

Here P_n is the matrix element of carrier-LO phonon scattering in QW used for the Huang-Rhys factor calculation, which is calculated as [58]:

$$\left| P_n\left(k_{\parallel} k_{\parallel}', jj'\right) \right|^2 / (\hbar\omega_{LO})^2 = \sum_q \overbrace{\frac{e^2}{2V_0\hbar\omega_{LO}} \left(\frac{1}{\varepsilon_\infty} - \frac{1}{\varepsilon_0}\right) \frac{q^2}{\left(q^2 + \lambda_s^2\right)} \delta\left(k_{\parallel} - k_{\parallel}', q_{\parallel}\right) \begin{Bmatrix} n_q + 1 \\ n_q \end{Bmatrix} \times \left| \int \phi_{nj}^*(z) \phi_{nj}(z) \exp(-iq_z) dz \right|^2}^{S_{ij}} \quad \text{(A5)}$$

where q_z is the phonon wave vector, $\boldsymbol{\varepsilon}_\infty$ is the optical dielectric constants, and V_0 is the system volume. The intraband relaxation time $\tau_{in} = \hbar / [\Gamma_{cjk_{\square}}(E) + \Gamma_{vjk_{\square}}(E)]$ is obtained from Eqs. (A1) and (A4).

REFERENCES

[1] Y. Zhao et al. *Toward High Efficiency at High Temperatures: Recent Progress and Prospects on InGaNBased Solar Cells*. Mater. Today Energy. 31 (2023) 101229. Available DOI:10.1016/j.mtener.2022.101229.

[2] S. Nakamura, T. Mukai, M. Senoh. *Candela-class high-brightness InGaN/AlGaN double-heterostructure blue-light-emitting diodes.* Appl. Phys. Lett. 64 (1994) 1687–1689. Available DOI:10.1063/1.111832.

[3] K. Fu, H. Fu, X. Huang, H. Chen, T.-H. Yang, J. Montes, C. Yang, J. Zhou, Y. Zhao. *Demonstration of 1.27 kV etch-then-regrow GaN p-n junctions with low leakage for GaN power electronics*. IEEE Electron Device Lett. 40(11) (2019) 1728. Available DOI: 10.1109/LED.2019.2941830.

[4] Y. Zhao, H. Fu, G. T. Wang, S. Nakamura.*Toward ultimate efficiency: progress and prospects on planar and 3D nanostructured nonpolar and semipolar InGaN light-emitting diodes*. Adv Opt Photonics. 10(1) (2018) 246. Available DOI:10.1364/AOP.10.000246.

[5] Z. Chen et al. *Positive temperature coefficient of photovoltaic efficiency in solar cells based on InGaN/GaN MQWs*. Appl. Phys. Lett. 109 (2016) 062104. Available DOI:10.1063/1.4960765

[6] L. Zhao, T. Detchprohm, C. Wetzel. *High 400°C operation temperature blue spectrum concentration solar junction in GaInN/GaN*. Appl. Phys. Lett. 105(24) (2014) 243903. Available DOI:10.1063/1.4904717.

[7] J. Wu, W. Walukiewicz, K. M. Yu, W. Shan, J. W. Ager. *III Superior radiation resistance of In $_{1-X}$Ga $_X$N alloys: Full-solar-spectrum photovoltaic material system*. J. Appl. Phys. 94(10) (2003) 6477. Available DOI:10.1063/1.1618353.

[8] C. J. Neufeld et al. *Observation of positive thermal power coefficient in InGaN/GaN quantum well solar cells*. Appl. Phys. Lett. 99 (2011) 071104. Available DOI: 10.1063/1.3624850.

[9] J. J. Williams et al. *Refractory $In_xGa_{1-x}N$ Solar Cells for High-Temperature Applications*. IEEE J. Photovolt. 7(6) (2017) 1646. Available DOI: 10.1109/JPHOTOV.2017.2756057.

[10] X. Huang, et al. *Reliability analysis of InGaN/GaN multi-quantum-well solar cells under thermal stress*. Appl. Phys. Lett. 111(23) (2017) 233511. Available DOI: 10.1063/1.5006650.

[11] A. Hangleiter. *Recombination dynamics in GaInN/GaN quantum wells*. Semicond. Sci. Technol. 34(7) (2019) 073002. Available DOI:10.1088/1361-6641/ab2788.

[12] J. Piprek. *Effciency Models for GaN-Based Light-Emitting Diodes: Status and Challenges*. Mater. 13 (2020)5174. DOI:10.3390/ma13225174.

[13] Q.H Pham, J. C Chen, H. B Nguyen. *Three-Dimensional Numerical Study on the Efficiency Droop in InGaN/GaN Light-Emitting Diodes*. IEEE Photonics J. 11(1) (2019) 8200417. Available DOI: 10.1109/JPHOT.2019.2893198.

[14] H.-Y Ryu, G.-H Ryu., Y.-H. Choi., B. Ma. *Modeling and simulation of efficiency droop in GaN-based blue lightemitting diodes incorporating the effect of reduced active volume of InGaN quantum wells*. Curr. Appl. Phys. 17 (2017) 1298-1302. Available DOI: 10.1016/j.cap.2017.06.014.

[15] A. Herzog, M. Wagner, T. Q. Khanh. *Efficiency droop in green InGaN/GaN light emitting diodes: Degradation mechanisms and initial characteristics*. Microelectron. Reliab. 112 (2020) 113792. Available DOI: 10.1016/j.microrel.2020.113792.

[16] T. Jeong, Hyung-Jo Park, Ju. Jin-Woo, H. Oh, J. Baek, J. Ha, G. Ryu, H. Ryu. *High efficiency InGaN blue light-emitting diode with >4-W output power at 3 A*. IEEE Photonics Technol. Lett. 26(7) (2014) 649. Available DOI: 10.1109/LPT.2014.2301874.

[17] G. Verzellesi, D. Saguatti, D. Saguatti, M. Meneghini, F. Bertazzi, M. Goano, G. Meneghesso, E. Zanoni. *Efficiency droop in InGaN/GaN blue light-emitting diodes: Physical mechanisms and remedies.* J. Appl. Phys. 114(7) (2013) 071101. Available DOI: 10.1063/1.4816434.

[18] Q. Dai et.al. *Carrier recombination mechanisms and efficiency droop in GaInN/GaN light-emitting diodes*. Appl. Phys. Lett. 97 (2010) 133507. Available DOI: 10.1063/1.3493654.

[19] H.-Y. Ryu, H.-S. Kim, J.-In Shim. *Rate equation analysis of efficiency droop in InGaN light-emitting diodes*. Appl. Phys. Lett. 95 (2009) 081114. Available DOI:10.1063/1.3216578.
[20] C. Onwukaeme, B. Lee, H.-Y. Ryu. *Temperature Dependence of Electron Leakage Current in InGaN Blue Light-Emitting Diode Structures*. Nanomater. 12 (2022) 2405. Available DOI:10.3390/nano12142405.
[21] J. Piprek, F. Römer, B. Witzigmann. *On the uncertainty of the Auger recombination coefficient extracted from InGaN/GaN light-emitting diode efficiency droop measurements*. Appl. Phys. Lett., 106 (2015) 101101. Available DOI:10.1063/1.4914833.
[22] R. Yahyazadeh. *Effect of hydrostatic pressure on the radiative current density of InGaN/GaN multiple quantum well light emitting diodes*. Opt. Quantum Electron. 53 (2021) 571. Available DOI:10.1007/s11082-021-03236-9.
[23] R. Yahyazadeh, Z. Hashempour. *Numerical investigation of Auger current density in a InGaN/GaN multiple quantum well solar cell under hydrostatic pressure*. Indian J. Phys. 98 (2024) 1217. Available DOI:10.1007/s12648-023-02897-4.
[24] J. Piprek. *Efficiency droop in nitride-based light-emitting diodes*. Phys. Status Solidi (A) Appl. Mater. Sci. 207(10) (2010) 2217. Available DOI:10.1002/pssa.201026149.
[25] W. Liu. *Shockley–Read–Hall recombination and efficiency droop in InGaN/GaN multiple-quantum-well green light-emitting diodes*. J. Phys. D Appl. Phys. 49 (2016) 145104. Available DOI: 10.1088/0022-3727/49/14/145104.
[26] A. David, N. G. Young, C. A. Hurni, M. D. Craven. *Quantum Efficiency of III-Nitride Emitters: Evidence for Defect-Assisted Nonradiative Recombination and its Effect on the Green Gap*. Phys. Rev. Appl. 11 (2019) 031001. Available DOI:10.1103/PhysRevApplied.11.031001.
[27] A. David, C. A. Hurni, N. G. Young, M. D. Craven. *Field-assisted Shockley-Read-Hall recombinations in III-nitride quantum wells*. Appl. Phys. Lett. **111** (2017) 233501. Available DOI:10.1063/1.5003112.
[28] M. Pristovsek, A. Bao, R. A. Oliver. *Effects of Wavelength and Defect Density on the Efficiency of (In,Ga)N-Based Light-Emitting Diodes*. Phys. Rev. Appl. **7** (2017) 064007. Available DOI:10.1103/PhysRevApplied.7.064007.
[29] S. Shishehchi, A. Asgari, R. Kheradmand. *The effect of temperature on the recombination rate of AlGaN/GaN light emitting diodes*. Opt. Quantum Electron. 41 (2009) 525. Available DOI:10.1007/s11082-009-9353-7.
[30] K.A. Bulashevich, V.F. Mymrin, S. Y. Karpov, I.A. Zhmakin, A. I. Zhmakin. *Simulation of visible and ultra-violet group-III nitride light emitting diodes*. J. Comput. Phys. 213(1) (2006) 214. Available DOI: 10.1016/j.jcp.2005.08.011.
[31] T. Suski et al. *A pressure-tuned blue-violet InGaN/GaN laser diode grown on bulk GaN crystal*. Appl. Phys. Lett. 84(8) (2004) 1236. Available DOI: 10.1063/1.1649801.
[32] A. Palma, A. Godoy, J. Jiménez-Tejada, J. Carceller, J. López-Villanueva. *Quantum two-dimensional calculation of time constants of random telegraph signals in metal-*

oxide–semiconductor structures. Phys. Rev. B Condens. 56(15) (1997) 9565. Available DOI: 10.1103/PhysRevB.56.9565.

[33] R. Yahyazadeh, Z. Hashempour. *Effect of hydrostatic pressure on the Auger coefficient of InGaN/GaN multiple-quantum-well laser diode.* J. Nanophotonics. 17(2) (2023) 026011. Available DOI: 10.1117/1.JNP.17.026011.

[34] X. Huang et al. *Piezo-Phototronic Effect in a Quantum Well Structure*. ACS Nano. 10(5) (2016) 5145. Available DOI: 10.1021/acsnano.6b00417.

[35] B. Jogai. *Influence of surface states on the two-dimensional electron gas in AlGaN/GaN heterojunction field-effect transistors*. J. Appl. Phys. 93 (2003) 1631. Available DOI: 10.1063/1.1530729.

[36] R. Yahyazadeh. *Effect of hydrostatic pressure on the photocurrent density of InGaN/GaN multiple quantum well solar cells*. Indian J. Phys. 96 (2022) 2815. Available DOI: 10.1007/s12648-021-02218-7.

[37] C. Xia, Z. Zeng, Q. Chang, S. Wei. *Donor impurity states in zinc-blende InGaN/GaN asymmetric coupled quantum dots: Hydrostatic pressure effect*. Phys. E: Low-Dimens. Syst. Nanostructures. 42(8) (2010) 2041. Available DOI: 10.1016/j.physe.2010.03.022.

[38] M. Usman. *Enhanced Internal Quantum Efficiency of Bandgap-Engineered GreenW-Shaped Quantum Well Light-Emitting Diode*. Appl. Sci. 9 (2019) 77. Available DOI: 10.3390/app9010077.

[39] J.Piprek, *Semiconductor Optoelectronic Devices: Introduction to Physics and Simulation*, Elsevier Science., San Diego, 2013, pp. 121–129.

[40] J. Nelson, *The Physics of Solar Cells*, Imperial College Press., London, 2003, pp.106-109.

[41] I. Vurgaftman, J. R. Meyer, L. R. Ram-Mohan. *Band parameters for III–V compound semiconductors and their alloys*. J. Appl. Phys. 89 (2001) 5815. Available DOI:10.1063/1.1368156.

[42] B. Chouchen et al. *Numerical modeling of InGaN/GaN p-i-n solar cells under temperature and hydrostatic pressure effects*. AIP Adv. 9 (2019) 045313. Available DOI:10.1063/1.5092236.

[43] A. Asgari, M. Kalafi, L. Faraone. *A quasi-two-dimensional charge transport model of AlGaN/GaN high electron mobility transistors (HEMTs)*. Phys. E: Low-Dimens. Syst. Nanostructures. 2**8**(4) (2005) 491. Available DOI: 10.1016/j.physe.2005.05.054.

[44] B. Jogai. *Parasitic Hole Channels in AlGaN/GaN Heterojunction Structures*. Phys. Status Solidi B Basic Res. 233(3) (2002) 506. Available DOI: 10.1002/1521-3951(200210)233:3<506: AID-PSSB506>3.0.CO;2-R.

[45] S. L. Chuang, C. S. Chang. *k.p method for strained wurtzite semiconductor*. Phys. Rev. B. 54 (1996) 2502. Available DOI:10.1103/PhysRevB.54.2491.

[46] S. Adachi, *Physical Properties of III-V compounds*, John Wiley & Sons., New York, 1992, pp.290.

[47] J. H. Zheng, H. S. Tan, S. C. Ng. *Theory of non-radiative capture of carriers by multiphonon processes for deep centres in semiconductors*. J. Phys.: Condens. Matter. 6(9) (1994) 1695. Available DOI: 10.1088/0953-8984/6/9/012.

[48] W. Wei-Ying et al. *Effects of interface roughness on photoluminescence full width at half maximum in GaN/AlGaN quantum wells*. Chin. Phys. B. 23(11) (2014) 117803. Available DOI: 10.1088/1674-1056/23/11/117803.

[49] J.G. Rojas-Briseño, I. Rodríguez-Vargas, M.E. Mora-Ramos, J.C. Martínez-Orozco. *Heavy and light exciton states in c-AlGaN/GaN asymm etric double quantum wells*. Phys. E: Low-Dimens. Syst. Nanostructures. 124 (2020) 114248. Available DOI: 10.1016/j.physe.2020.114248.

[50] B. K. Ridley, W. J. Schaff, and L. F. Eastman. *Theoretical model for polarization superlattices: Energy levels and intersubband transition*s. J. Appl. Phys. 94 (2003)3972. DOI:10.1063/1.1601686.

[51] Mi. Lozac'h, Y. Nakano, L. Sang, K. Sakoda, M. Sumiya. *Study of Defect Levels in the Band Gap for a Thick InGaN Film.* Jpn. J. Appl. Phys. 51(12) (2012) 121001. Available DOI: 10.1143/JJAP.51.121001.

[52] C.D. Vedel, T. Gunst, S. Smidstrup, V. P. Georgiev. *Shockley-Read-Hall recombination and trap levels in In0.53 Ga 0.47 As point defects from first principles*. Phys. Rev. B. 108 (2023) 094113. Available DOI: 10.1103/PhysRevB.108.094113.

[53] J. F. Kong, W. Z. Shen, Q. X. Guo. *Raman-scattering probe of anharmonic effects due to temperature and composition in InGaN*. Phys. Status Solidi B Basic Res, 250(2) (2013) 329. Available DOI:10.1002/pssb.201248374.

[54] X. D. Pu, J. Chen, W. Z. Shen, H. Ogawa, Q. X. Guo. *Temperature dependence of Raman scattering in hexagonal indium nitride films*. J. Appl. Phys. 98 (2005) 033527. Available DOI:10.1063/1.2006208.

[55] S. Kasap, P. Capper, *Springer Handbook of Electronic and Photonic Materials*, Springer., Cham, 2017, pp.725-727

[56] Xia, C., Zeng, Z., Chang, Q., Wei, S. *Donor impurity states in zinc-blende InGaN/GaN asymmetric coupled quantum dots: Hydrostatic pressure effect*. Phys. E: Low-Dimens. Syst. Nanostructures. 42, (2010). 2041. Available DOI:10.1016/j.physe.2010.03.022.

[57] S.P. Zory, *Quantum Well Lasers*, Academic Press., San Diego, California, 1993, pp. 58–150.

[58] B.K. Ridley. *A note on the origin of the yellow luminescence in GaN*." J. Phys.: Condens. Matter. 10(28) (1998) 461. Available DOI:10.1088/0953-8984/10/27/003.

[59] J. Wang, P. von Allmen, J.P. Leburton, K.J. Linden. *Auger recombination in long-wavelength strained-layer quantum-well structures*. IEEE J. Quantum Electron. 31(5) (1995) 864. Available DOI: 10.1109/3.375931.

[60] E. Kioupakis, D. Steiauf, P. Rinke, K. T. Delaney, C. G. Van de Walle1. *First-principles calculations of indirect Auger recombination in nitride semiconductors*. Phys. Rev. B. 92 (2015) 035207. Available DOI: 10.1103/PhysRevB.92.035207.

[61] Y. Q. Kang, J. H. Zheng, H. S. Tan, S. C. Ng. *Charge-state effects of deep canters semiconductors on non-radiative capture of carriers by multiphonon processes*. Appl. Phys. A. 63 (1996) 37. Available DOI: 10.1007/BF01579744.

[62] J. W. Pan, J.I. Chyi. *Theoretical Study of the Temperature Dependence of 1.3-pm AlGaInAs-InP Multiple-Quantum-Well Lasers*. IEEE J. Quantum Electron. 32(12) (1996) 2133. Available DOI: 10.1109/3.544760.

[63] R. Yahyazadeh, Z. Hashempour, *Non-radiative Auger Current in a InGaN/GaN Multiple Quantum Well Laser Diode under Hydrostatic Pressure and Temperature.* Journal of Optoelectronical Nanostructures. 8(2) (2023) 81-107. Available DOI: 10.30495/jopn.2023.31803.1289

[64] J. Wang, P. V. Allmen, J.-P. Leburton, K. J. Linden. *Auger Recombination in Long-Wavelength Strained-Layer Quantum-Well Structures*. IEEE J. Quantum Electron. 31(5) (1995) 864-875. Available DOI: 10.1109/3.375931.

[65] M. Amirhoseiny, G. Alahyarizadeh. *Enhancement of Deep Violet InGaN Double Quantum WellsLaser Diodes Performance Characteristics Using Superlattice Last Quantum Barrier*. Journal of Optoelectronical Nanostructures. 6(2) (2021) 107-120. Available DOI: 10.30495/jopn.2021.4776

[66] R. Yahyazadeh, Z. Hashempour, *Effect of Hydrostatic Pressure on Optical Absorption Coefficient of InGaN/GaN of Multiple Quantum Well Solar Cells.* Journal of Optoelectronical Nanostructures. 6(2) (2021) 1-22. Available DOI: 10.30495/jopn.2021.27941.1221

[67] R. Yahyazadeh, Z. Hashempour, *Numerical Modeling of Electronic and Electrical Characteristics of* $Al_{0.3}\ Ga_{0.7}\ N$ */ GaN Multiple Quantum Well Solar Cells*. Journal of Optoelectronical Nanostructures. 5(3) (2020) 81-101. Available DOR: 20.1001.1.24237361.2020.5.3.6.5

[68] Y. Li et al. *Effect of the band structure of InGaN/GaN quantum well on the surface plasmon enhanced light-emitting diodes*. J. Appl. Phys. 116 (2014) 013101. Available DOI: 10.1063/1.4886223.

[69] V. B. Yekta, H. Kaatuzian. *Design considerations to improve high temperature characteristics of 1.3μm AlGaInAs-InP uncooled multiple quantum well lasers: Strain in barriers*. Optik. 122 (2011) 514. Available DOI: 10.1016/j.ijleo.2010.03.016.

[70] A. Horri, S. Z. Mirmoeini. *Analysis of Kirk Effect in Nanoscale Quantum Well Heterojunction Bipolar Transistor Laser*. Journal of Optoelectronical Nanostructures. 5(2) (2020) 25-38. Available DOR: 20.1001.1.24237361.2020.5.2.3.0

[71] C.D. Mahan, Many-body particle physics. Plenum press, New York and London, Chap.3 (1990).

[72] R. Nagarajan et al. *High speed quantum-well lasers and carrier transport effects*. IEEE J. Quantum Electron. 28(10) (1992) 1990–2008. Available DOI: 10.1109/3.159508.

[73] Z. Jun, B. Shi-Liang, H. Si-Hua. *Phonon-assisted intersubband transitions in wurtzite* $GaN/In_x\ Ga_{1-X}\ N$ *quantum wells*. Chin. Phys. B. 21(9) (2012) 097301. Available DOI: 10.1088/1674-1056/21/9/097301.

[74] L. L. Guo, Y. H. Zhang, W. Z. Shen. *Temperature dependence of Raman scattering in GaMnN.* Appl. Phys. Lett. 89 (2006) 161920. Available DOI: 10.1063/1.2364472.

[75] X. Xiao-Yong et al. *Temperature dependences of Raman scattering in different types of GaN epilayers*. Chin. Phys. B. 21(2) (2012) 027803. Available DOI: 10.1088/1674-1056/21/2/027803.

[76] A. Link et al. *Temperature dependence of the E2 and A1(LO) phonons in GaN and AlN*. J. Appl. Phys. 86 (1999) 6256. Available DOI: 10.1063/1.371681.

[77] V. Fiorentini. *Evidence for nonlinear macroscopic polarization in III–V nitride alloy heterostructures*. Appl. Phys. Lett. 80 (2002) 1204. Available DOI: 10.1063/1.1448668.

[78] P. Perlin, L. Mattos, N. A. Shapiro, J. Kruger, W. S. Wong, T. Sands. *Reduction of the energy gap pressure coefficient of GaN due to the constraining presence of the sapphire substrate*. J. Appl. Phys. 85 (1999) 2385. Available DOI: 10.1063/1.369554.

[79] M. Zhang, P. Bhattacharya, J. Singh, and J. Hinckley. *Direct measurement of auger recombination in In0.1Ga 0.9N / GaN quantum wells and its impact on the efficiency of In0.1Ga 0.9N / GaN multiple quantum well light emitting diodes.* Appl. Phys. Lett. 95 (2009) 201108. Available DOI: 10.1063/1.3266520.

[80] Y. C. Shen, G. O. Mueller, S. Watanabe, N. F Gardner, A. Munkholm, M. R. Krames, "Auger recombination in InGaN measured by photoluminescence," Appl. Phys. Lett. 91 141101 (2007). Available DOI:10.1063/1.2785135.

[81] M. Meneghini, N. Trivellin, G. Meneghesso, E. Zanoni. U. Zehnder, B. Hahn. *A combined electro-optical method for the determination of the recombination parameters in InGaN-based light-emitting diodes*. . J. Appl. Phys. 106 (2009) 114508. Available DOI:10.1063/1.3266014.

[82] A. Laubsch, M. Sabathil, J. Baur, M. Peter, and B. Hahn. *High-Power and High-Efficiency InGaN-Based Light Emitters.* IEEE Trans. Electron Devices. 57(1), (2010) 79. Available DOI: 10.1109/TED.2009.2035538.